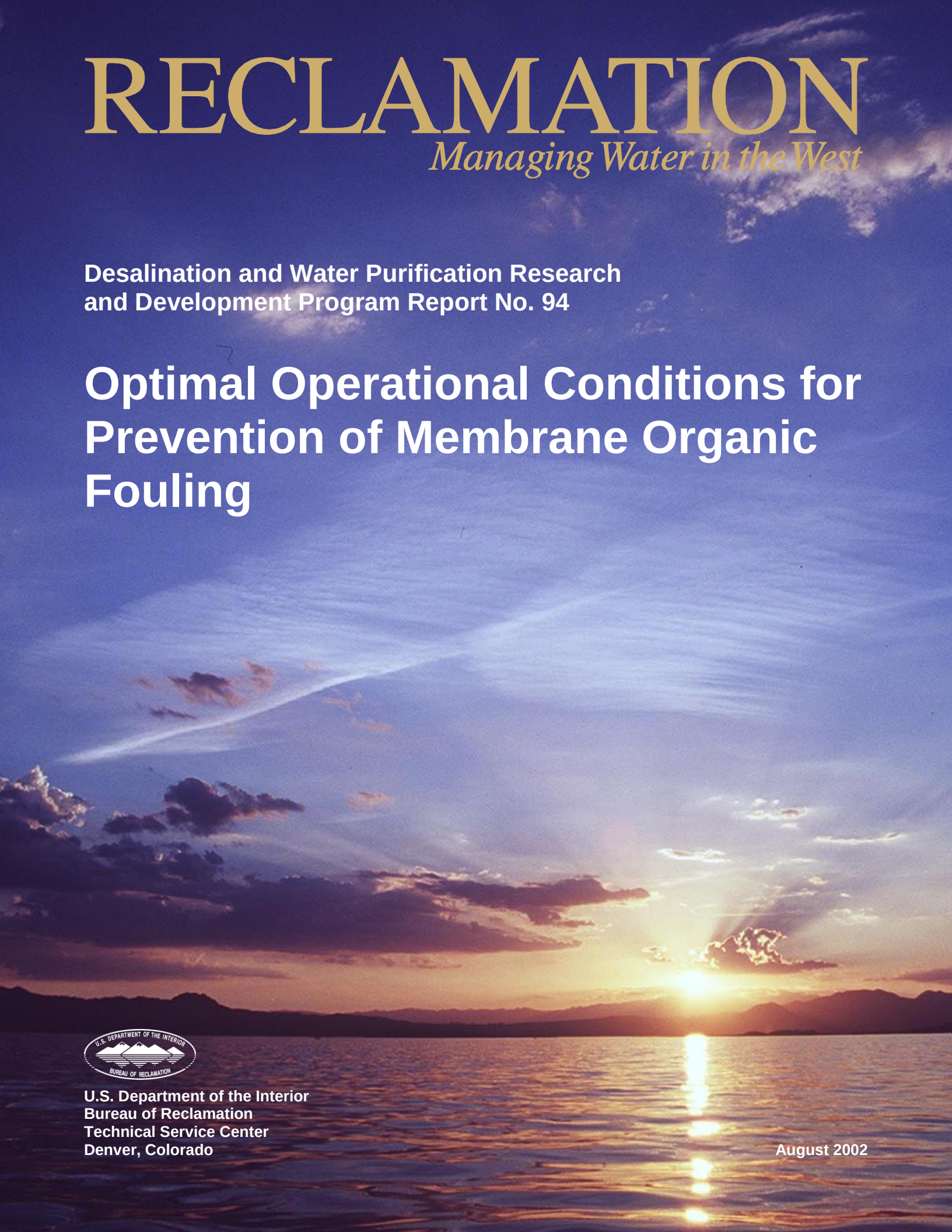

RECLAMATION

Managing Water in the West

Desalination and Water Purification Research and Development Program Report No. 94

Optimal Operational Conditions for Prevention of Membrane Organic Fouling

U.S. Department of the Interior
Bureau of Reclamation
Technical Service Center
Denver, Colorado

August 2002

REPORT DOCUMENTATION PAGE

Form Approved
OMB No. 0704-0188

1. REPORT DATE *(DD-MM-YYYY)*	2. REPORT TYPE	3. DATES COVERED *(From - To)*
August 2002	Final	October 1999 to August 2002

4. TITLE AND SUBTITLE
Optimal Operational Conditions for Prevention of Membrane Organic Fouling

5a. CONTRACT NUMBER
Agreement No 99-FC-81-0187

5b. GRANT NUMBER

5c. PROGRAM ELEMENT NUMBER

6. AUTHOR(S)
Menachem Elimelech

5d. PROJECT NUMBER

5e. TASK NUMBER
Task A

5f. WORK UNIT NUMBER

7. PERFORMING ORGANIZATION NAME(S) AND ADDRESS(ES)
Yale University

8. PERFORMING ORGANIZATION REPORT NUMBER

9. SPONSORING/MONITORING AGENCY NAME(S) AND ADDRESS(ES)
Bureau of Reclamation
U.S. Department of the Interior
Denver Federal Center
PO Box 25007, Denver, CO 80225-0007

10. SPONSOR/MONITOR'S ACRONYM(S)
Reclamation

11. SPONSOR/MONITOR'S REPORT NUMBER(S)
DWPR Report No. 94

12. DISTRIBUTION/AVAILABILITY STATEMENT
Available from the National Technical Information Service,
Operations Division, 5285 Port Royal Road, Springfield VA 22161

13. SUPPLEMENTARY NOTES
Report can be downloaded from Reclamation Web site: http://www.usbr.gov/pmts/water/publications/reports.html

14. ABSTRACT

A systematic investigation on the role of hydrodynamics (initial permeate flux and crossflow rate) and divalent cations (calcium) in natural organic matter fouling of nanofiltration (NF) membranes was carried out. Results showed that membrane fouling and performance are governed by the coupled influence of chemical and hydrodynamic interactions. Permeation drag and calcium binding to organic matter cause development of a densely compacted fouling layer on the membrane surface. An increase in crossflow velocity mitigates these effects to some extent. Natural organic matter (NOM) fouling of NF membranes is governed by the combined influence of initial permeate flux, crossflow velocity, and divalent ion concentration. Permeation drag (controlled by permeate flux) and calcium binding to NOM are the major cause for the observed rapid flux decline. An increase in crossflow velocity lessens these effects by reducing NOM deposition on the membrane surface and arresting the growth of the NOM fouling layer. The results clearly demonstrate the coupling between the hydrodynamic characteristics (permeation drag and shear rate) and chemical reactions that are involved in NOM fouling of crossflow NF systems. For a given solution composition, proper choice of initial flux and crossflow rate can improve membrane performance and reduce operating costs.

15. SUBJECT TERMS
Organic Fouling, Nanofiltration, Membranes

16. SECURITY CLASSIFICATION OF:			17. LIMITATION OF ABSTRACT	18. NUMBER OF PAGES	19a. NAME OF RESPONSIBLE PERSON
			SAR		Frank Leitz
a. REPORT	b. ABSTRACT	a. THIS PAGE			19b. TELEPHONE NUMBER *(Include area code)*
U	U	U			303-445-2255

Desalination and Water Purification Research and Development Program Report No. 94

Optimal Operational Conditions for Prevention of Membrane Organic Fouling

Prepared for the Bureau of Reclamation Under Agreement No. 99-FC-81-0187

by

Menachem Elimelech
Department of Chemical Engineering
Environmental Engineering Program
Yale University, New Haven, Connecticut

U.S. Department of the Interior
Bureau of Reclamation
Technical Service Center
Denver, Colorado

August 2002

MISSION STATEMENTS

The U.S. Department of the Interior protects America's natural resources and heritage, honors our cultures and tribal communities, and supplies the energy to power our future.

The mission of the Bureau of Reclamation is to manage, develop, and protect water and related resources in an environmentally and economically sound manner in the interest of the American public.

Disclaimer

The views, analysis, recommendations, and conclusions in this report are those of the authors and do not represent official or unofficial policies or opinions of the United States Government, and the United States takes no position with regard to any findings, conclusions, or recommendations made. As such, mention of trade names or commercial products does not constitute their endorsement by the United States Government.

Acknowledgments

This research was funded by the U.S. Department of the Interior, Bureau of Reclamation, Desalination and Water Purification Research and Development Program.

CONTENTS

Figures

ACRONYMS AND ABBREVIATIONS

ACS	American Chemical Society
°C	degrees Celsuis
cm/s	centimeters per second
cm^2	square centimeters
g	gram
kPa	kilopascal
L	liters
M	moles per liter
mg/L	milligrams per liter
mM	millimoles per liter
NF	nanofiltration
NOM	natural organic matter
TOC	total organic carbon
TDS	total dissolved solids
UV	ultraviolet light
µM	micromoles per liter
µm/s	micrometers per second

EXECUTIVE SUMMARY

A systematic investigation on the role of hydrodynamics (initial permeate flux and crossflow rate) and divalent cations (calcium) in natural organic matter (NOM) fouling of nanofiltration (NF) membranes is reported. Fouling experiments with a thin-film composite NF membrane were conducted in a bench-scale, crossflow unit at various combinations of calcium ion concentration, initial permeate flux, and crossflow velocity. Results showed that membrane fouling and performance are governed by the *coupled* influence of chemical and hydrodynamic interactions. Permeation drag and calcium binding to NOM are the major cause for the development of a densely compacted fouling layer on the membrane surface, which leads to severe flux decline. An increase in shear rate (crossflow velocity) mitigates these effects to some extent by reducing the transport of NOM toward the membrane and arresting the growth of the fouling layer. The pronounced coupled influence of the initial permeate flux and crossflow velocity on the membrane fouling behavior suggests fouling control via optimization of these parameters, thus enabling high product water flux at reduced operational costs.

1 INTRODUCTION

Fouling is a major obstacle for efficient use of membrane technology for treatment of natural waters. Membrane fouling results in deterioration of membrane performance (i.e., permeate flux and quality) and ultimately shortens membrane life. Among the many potential foulants that are ubiquitous in natural waters, natural organic matter (NOM) is one of the most recalcitrant. Therefore, understanding the causes of membrane fouling by NOM and developing strategies for fouling control are major challenges.

The rate and extent of membrane fouling are influenced by operating conditions, such as the applied pressure and crossflow velocity [1–11]. Among the different physical parameters governing the extent and severity of fouling, the most important is the applied pressure. Applied pressure governs the initial permeate flux and the resulting convective transport of foulants toward the membrane surface. Higher permeate flux results in severe fouling due to higher permeation drag and more compressed foulant layers [1, 10]. Thus, although higher operating pressures allow for higher initial permeate flux, the following rapid decline in flux may counteract this advantage.

In addition to physical parameters, solution chemistry (pH and ionic composition) plays a significant role in determining foulant-foulant and foulant-membrane electrostatic double layer interactions and hence membrane performance [1, 8, 12, 13]. For NOM, solution chemistry also controls the charge and configuration of NOM macromolecules and hence the structure and hydraulic resistance of the foulant deposit layer. Multivalent cations, such as calcium and magnesium, react with NOM to form Ca-NOM complexes, which results in a highly compacted fouling layer and severe flux decline [1, 4, 7, 12, 13].

Recent work on colloidal and NOM fouling reveals that the rate of foulant attachment (deposition) onto a membrane surface and subsequent fouling are controlled by a delicate interplay (coupling) between electrostatic double layer repulsion and the opposing hydrodynamic force (permeation drag), which is proportional to the convective permeate flow toward the membrane [1, 13]. Under typical operating conditions, the permeation drag can be significant, overcoming the opposing electrostatic double layer repulsive force and resulting in foulant deposition and subsequent membrane fouling. At low permeate flux, on the other hand, the repulsive electrostatic double layer forces may be strong enough to hinder foulant attachment onto the membrane.

While the above results point out to the important roles of hydrodynamics (permeate flux) and chemical interactions (electrostatic double layer repulsion and Ca-NOM complexation), there is a need for a more systematic investigation of the interplay between these forces, at various solution chemistries and initial permeate fluxes. Furthermore, the above studies were conducted at a fixed crossflow velocity; the latter may have an important effect on membrane fouling. The main objective of this work was to systematically investigate the *coupled* influence of calcium ion concentration, initial permeate flux, and crossflow velocity in controlling NOM fouling of NF membranes in a bench-scale crossflow set-up. The mechanisms for the coupled influence of chemical and hydrodynamic interactions on NOM fouling are delineated and the implications for optimization of operational parameters for fouling control are evaluated and discussed.

2 MATERIALS AND METHODS

2.1 Reagents and Model NOM

Deionized water (Nanopure Infinity Ultrapure, Barnstead, Dubuque, Iowa) was used for preparation of all stock solutions and for membrane fouling and performance experiments. American Chemical Society (ACS) grade NaCl, $CaCl_2 \cdot 2H_2O$, and $NaHCO_3$ salts, as well as trace metal sodium hydroxide and hydrogen chloride, were obtained from Fisher (Pittsburgh, Pennsylvania).

The commercial humic acid (Aldrich, Milwaukee, Wisconsin), chosen as model NOM, was purified via repeated precipitation with hydrochloric acid to remove bound iron and decrease the ash content as described in Hong and Elimelech [1]. The NOM was characterized for its total organic carbon (TOC) content (TOC-5000A, Shimadzu, Kyoto, Japan) using potassium hydrogen phthalate (Accustandard, New Haven, Connecticut) as a standard. The model NOM carbon content was determined to be 0.445 gram (g) TOC/g NOM, in accord with reported data values for various natural waters [14]. Other properties of the NOM are reported elsewhere [1].

2.2 NF Membrane

The relatively well characterized and documented thin film composite NF-70 (Dow-FilmTec, Minnetonka, Minnesota) was used as a model NF membrane in the fouling experiments. The membrane was characterized for surface morphology and charge properties via atomic force microscopy and streaming potential measurements, respectively, as described elsewhere [9]. Pure water permeability was determined after the membrane was equilibrated for 24 hours with deionized water at 1,034 kilopascal (kPa) and a crossflow velocity of 12.1 centimeters per second (cm/s). When a steady flux was achieved the pressure was incrementally reduced from the initial value of 1034 kPa down to 345 kPa, and the permeate flux was monitored at each pressure, from which a permeability of 3.06×10^{-11} m s^{-1} Pa^{-1} was calculated.

2.3 Crossflow Membrane Test Unit

A typical laboratory scale crossflow membrane test unit was employed for the fouling runs. The unit consisted of two parallel rectangular plate-and-frame membrane cells, with each cell having a membrane surface area of 20.0 square centimeters (cm^2) (2.6 × 7.7 cm) and a cross-sectional flow area of 0.78 cm^2. The system was operated in a closed loop mode in which both permeate and retentate were recirculated into the 20-liters (L) feed solution reservoir. The magnetically stirred feed solution was pumped to the membrane cells using a high-pressure pump (Hydracell pump, Wanner Engineering, Minneapolis, Minnesota). A back-pressure regulator (U.S. Paraplate, Auburn, California) in conjunction with a by-pass valve (Swagelok, Solon, Ohio) at the entrance allowed fine control of the applied pressure and crossflow velocity, respectively. Temperature was maintained at 25 degrees celsuis (°C) by a recirculating heater/chiller (Model 633, Polysciences), retentate flow rate was monitored by a floating disc rotameter (King Instruments, Fresno, California), and the permeate flux was monitored continuously by a digital flowmeter (Optiflow 1000, J&W Scientific Inc., Folsom, California) interfaced with a personal computer. More details on the NF system and its operation are given in our previous publication [1].

2.4 Fouling Experiments

NOM fouling experiments were performed using the above-described test unit equipped with the thin-film composite NF-70. The model feed solution contained 20 milligrams per liter (mg/L) humic acid, 10^{-3} *M* sodium bicarbonate, and up to 1 millimoles per liter (m*M*) Ca^{2+} as calcium chloride. In all fouling experiments, the feed solution temperature was kept at 25 °C, the solution pH was maintained at 8±0.1, and the total ionic strength was fixed at 0.01 moles per liter (*M*) (adjusted by sodium chloride). NOM fouling runs were performed for various combinations of calcium ion concentration, initial permeate flux, and crossflow velocity.

The experimental protocol for the fouling experiments was as follows. The membrane was first equilibrated for 20 hours with deionized water at 1,034 kPa and a crossflow velocity of 12.1 cm/s, and then with NOM-free electrolyte solution for approximately 5 hours, at the pressure and crossflow velocity to be used in the subsequent fouling test. After a steady permeate flux was achieved, the fouling test was initiated by the addition of an appropriate volume of concentrated NOM stock solution to the feed solution. The fouling run was continued for 50 hours, during which the permeate flux was continuously monitored. Samples from the feed and permeate solutions were taken periodically to determine NOM, total dissolved solids (TDS), and Ca^{2+} rejection.

At the end of the fouling run, the membranes were carefully removed from the cells, and both membranes were photographed. The deposited mass of NOM on the fouled membrane surface was quantified gravimetrically according to the procedure described in Hong and Elimelech [1]. The test unit was then thoroughly cleaned to remove any remaining NOM by recirculating sodium hydroxide solution (pH 11) followed by deionized water.

2.5 Rejection Analyses

Rejections of TDS, Ca^{2+}, and NOM were determined from the measured feed and permeate concentrations of samples collected during the course of the fouling tests. Conductivity measurements (YSI Model 32, YSI Co., Inc., Yellow Springs, Ohio) were used to determine TDS rejection. Calcium was measured using an ion-selective-electrode (ISE model 93-20 with 90-01 reference electrode, Orion Research Inc., Boston, Massachusetts), and UV absorbance at 254 nm (Hewlett Packard 8453) was used to measure NOM.

3 RESULTS AND DISCUSSION

3.1 Influence of Hydrodynamic Conditions on Fouling

3.1.1 Initial Permeate Flux

The effect of initial permeate flux on the NOM fouling behavior at different crossflow velocities is shown in Figure 1. For each set of experiments, the fouling behavior is plotted in two different forms, namely flux versus time (top, Figures 1a–c) and the corresponding normalized flux versus cumulative permeate volume (bottom, Figures 1d–e). A greater flux decline is observed for higher initial fluxes, thus confirming our previous finding regarding the paramount role of the applied pressure, the driving force for the filtration process, in membrane fouling [1, 15, 16]. For a given solution composition and crossflow velocity, a greater rate of flux decline is noticed at the early stages of filtration when the permeate flux is high; however, the permeate fluxes appear to converge to a limiting value irrespective of the initial flux. This is clearly illustrated in Figure 1a for the lowest crossflow velocity (4.0 cm/s, corresponding to a Reynolds

number of 217) where all three permeate fluxes converged within the 50 hours of the run. A similar result, to a lesser extent, is seen in Figures 1b and 1c for the higher crossflow velocities (12.1 and 40.4 cm/s or Reynolds numbers of 656 and 2170, respectively). In Figure 1c, only the fouling curves at the two higher initial fluxes (11.3 and 16.9 μm/s) converged within the timeframe of the run; therefore, further fouling and flux decline would be expected for these runs before a (pseudo) steady state is reached.

Although operation at a high initial permeate flux may appear desirable for obtaining high quantities of product water from a given membrane system, the dramatic flux decline most likely offsets this benefit due to excessive fouling. Fouling not only increases operational costs by increasing energy demand but may also cause severe damage to the membrane in the long run. As shown in Figure 1, NOM fouling can be nearly prevented for the runs at the lowest permeate flux (5.6 micromoles per liter [μm/s]). This implies that the runs at this low initial flux were performed near or below the critical flux. Further discussion on the economic consequences of fouling and the importance of optimizing operational parameters is given in Section 3.5.

Fouling of NF membranes by NOM macromolecules is attributed to the increase in hydraulic resistance due to the accumulated NOM fouling layer at the membrane surface [1, 4, 8, 10]. Higher convective transport of NOM toward the membrane at higher initial fluxes inevitably results in greater deposition of rejected NOM. However, as can be clearly seen in Figures 1d–1e, the greater NOM transfer rate at the higher initial flux is not sufficient to explain the difference in the fouling curves, as there is still a large difference in the rate and extent of flux decline at similar accumulated permeate volumes. The observed effect of initial flux on the NOM fouling behavior is mainly attributed to the permeation drag resulting from the convective flow toward the membrane. As discussed in our previous publications [1, 15, 16], this hydrodynamic force acting on the transported NOM macromolecules can overcome the electrostatic repulsion between the NOM and the membrane, thus resulting in NOM deposition. In addition to the above effect of permeation drag, increased fouling can be associated with the elevated concentration of rejected Ca^{2+} at the membrane surface due to concentration polarization. This effect is described later in Section 3.3.2. Lastly, fouling layers formed at higher applied pressures are expected to be more compact, thus further enhancing flux decline.

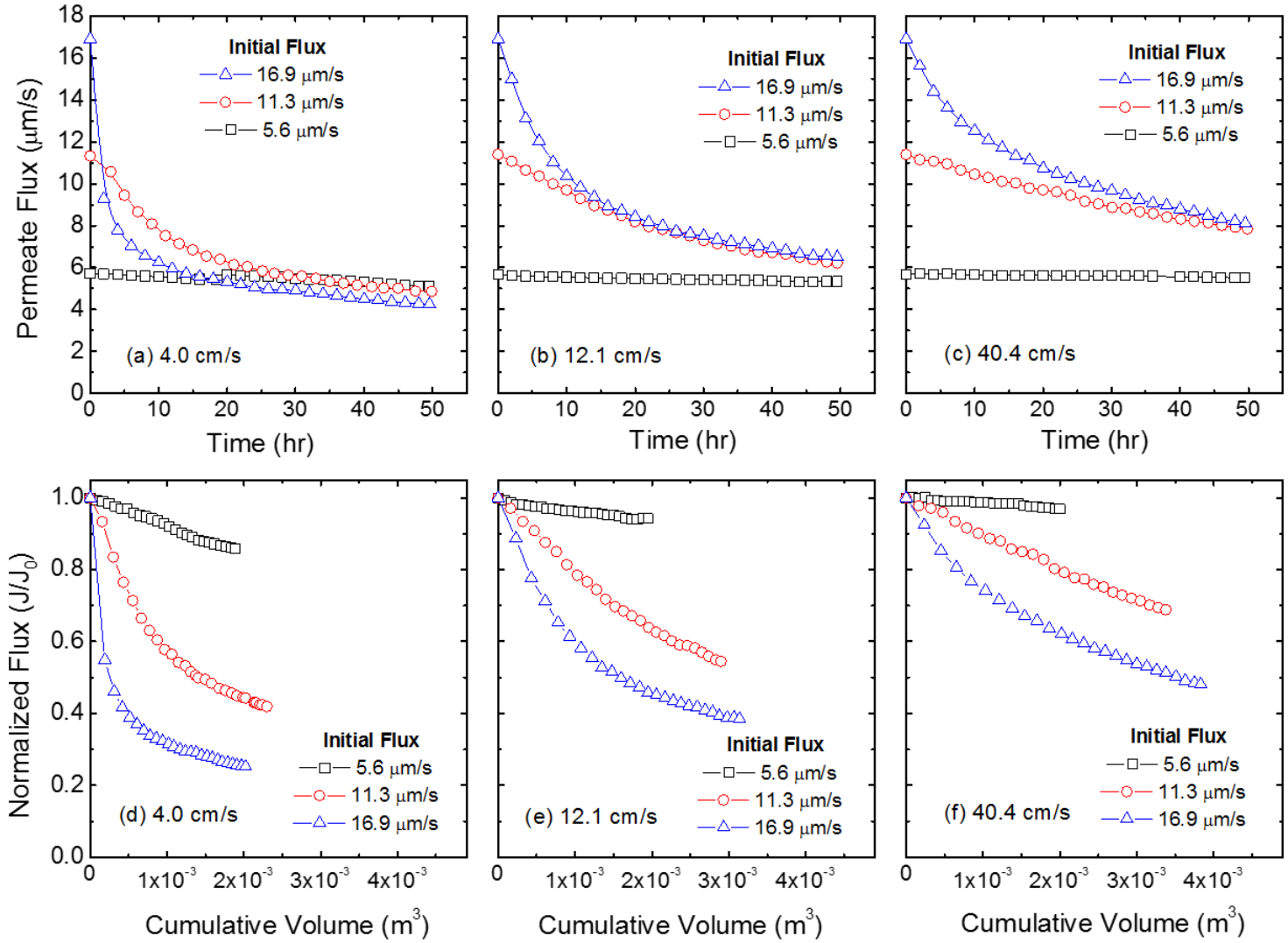

Figure 1. Effect of initial permeate flux on NOM fouling for various crossflow velocities.

Results are presented as flux versus time for crossflow velocities of (a) 4.0 cm/s, (b) 12.1 cm/s, and (c) 40.4 cm/s. The corresponding fouling curves presented as normalized flux (J/J_0) versus cumulative volume are shown below the flux versus time curves for crossflow velocities of: (d) 4.0 cm/s, (e) 12.1 cm/s, and (f) 40.4 cm/s. The following conditions were maintained during the fouling experiments: 0.3 m*M* Ca^{2+} (as $CaCl_2$), 1.0 m*M* $NaHCO_3$, total ionic strength of 10 m*M* (adjusted by adding 8.1 m*M* NaCl), pH 8.0±0.1, and temperature of 25 °C.

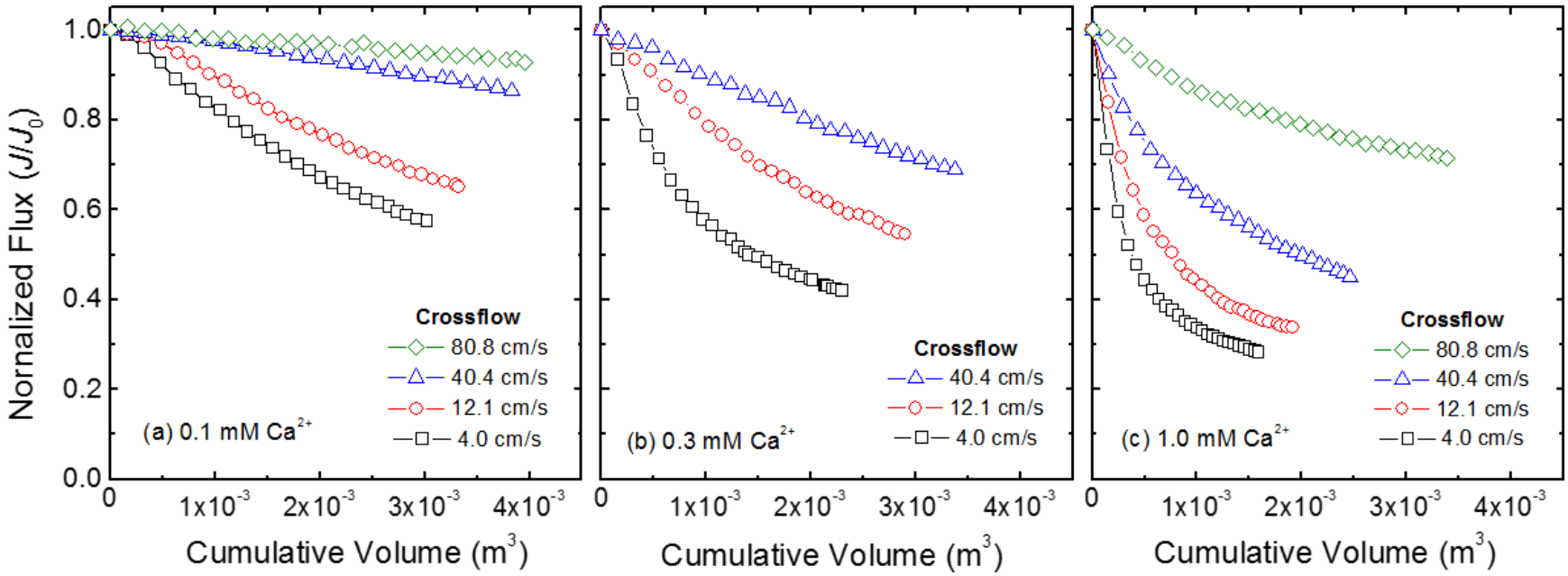

Figure 2. Effect of crossflow velocity on NOM fouling at various calcium ion concentrations.

Results are presented as normalized flux (J/J_0) versus cumulative volume for calcium ion concentrations of (a) 0.1 m*M*, (b) 0.3 m*M*, and (c) 1.0 m*M*. The following conditions were maintained during the fouling experiments: initial permeate flux (J_0) of 11.3 μm/s, 1.0 m*M* $NaHCO_3$, total ionic strength of 10 m*M* (adjusted by adding NaCl), pH 8.0±0.1, and temperature of 25 °C.

3.1.2 Crossflow Velocity

The influence of crossflow velocity on NOM fouling is illustrated in the fouling curves presented in Figure 1. The results demonstrate the significant impact of crossflow velocity on reducing the rate of flux decline that is always associated with membrane filtration at high initial permeate fluxes. For instance, it is shown that at the highest initial permeate flux employed (16.9 μm/s) the flux after 50 hours of operation is twice as large when the crossflow velocity is increased by a factor of 10 (from 4.0 to 40.4 cm/s). This effect, however, diminishes as the initial permeate flux decreases.

Additional fouling runs investigating the important role of crossflow velocity on NOM fouling are shown in Figure 2 for a fixed initial permeate flux (11.3 μm/s) and various Ca^{2+} concentrations (0.1, 0.3, and 1.0 m*M*). For example, the observed flux decline at the highest crossflow velocity (80.8 cm/s) after 50 hours is approximately 28 and 7 percent for 1.0 and 0.1 m*M* calcium concentration, respectively, whereas the corresponding decline for the lowest crossflow velocity (4.0 cm/s) was as much as 72 and 43 percent (Figures 2a and 2c). The effect of crossflow velocity on NOM fouling is attributed to the increase in shear rate and the resulting reduction in NOM deposition/accumulation at the membrane surface. In addition, as we discuss later, increased fouling at low crossflow rates can be associated with the elevated concentration of rejected Ca^{2+} at the membrane surface due to enhanced concentration polarization. Further, the contribution of crossflow to reducing fouling is dependent on both the initial flux and calcium concentration, and these coupled effects are discussed in Section 3.3.

3.2 Influence of Divalent (Calcium) Ion Concentration on Fouling

Recent studies have demonstrated that divalent cations, such as Ca^{2+} and Mg^{2+}, have a dramatic effect on NOM fouling of pressure-driven membranes [1, 4, 8, 10]. The fouling data presented in Figure 2 clearly show that the rate and extent of NOM fouling significantly increase as calcium ion concentration increases. Additional fouling data at various calcium ion concentrations are shown in Figure 3. It is evident that, at high initial flux, fouling becomes more severe as calcium ion concentration increases. Permeate flux, however, is nearly independent of calcium concentration (at the tested range) at the lowest initial flux (5.6 micrometers per second [μm/s], Figure 3c), as such low flux is not conducive for membrane fouling.

The important role of calcium in NOM fouling is attributed to the specific binding (complexation) of the divalent calcium ions to acidic functional groups of NOM [1]. Such specific interactions of calcium ions result in a compact and highly resistant fouling layer at the membrane surface, which leads to severe flux decline. Bridging within the deposited NOM due to Ca-NOM complexation further enhances the compactness of the fouling layer [1]. As pointed out by Hong and Elimelech [1], the specific resistance of a cake/gel layer formed in the presence of divalent cations is much higher than the case

with monovalent cations. The compact structure of the fouling layer—rather than simply the NOM deposit mass—governs the flux decline during NOM fouling.

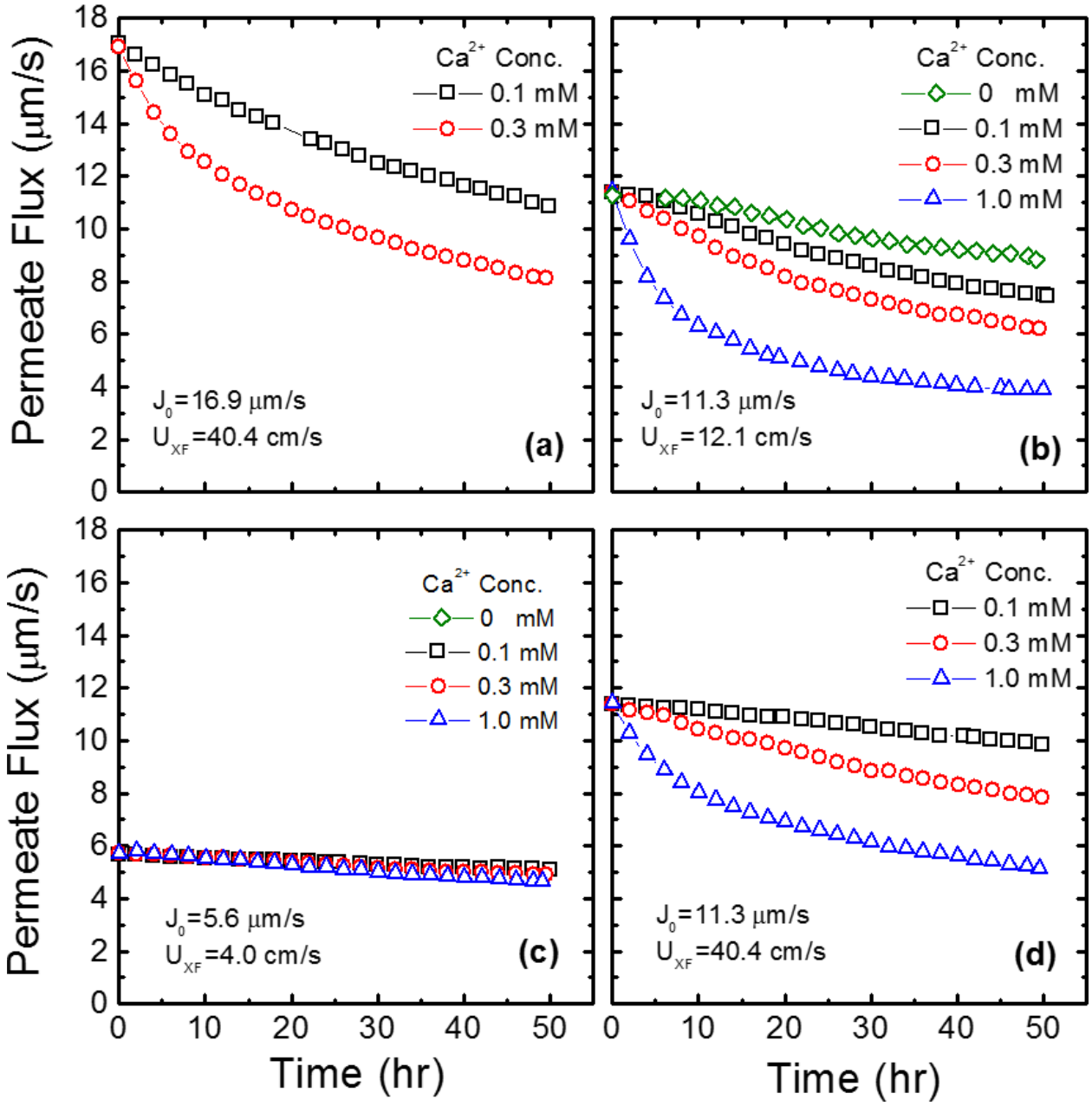

Figure 3. Effect of calcium ion concentration on membrane fouling at different hydrodynamic conditions (crossflow velocities, U_{XF}, and initial fluxes, J_0, as indicated in the figure).
The following conditions were maintained during the fouling experiments: 1.0 m*M* $NaHCO_3$, total ionic strength of 10 m*M* (adjusted by adding NaCl), pH 8.0±0.1, and temperature of 25 °C.

3.3 Combined Influence of Physical and Chemical Interactions

3.3.1 The NOM Fouling Layer

Typical snapshots of fouled membranes are shown in Figure 4. The remarkable effect of hydrodynamic and chemical conditions on the accumulation of NOM on the membrane is obvious. Under highly conducive conditions for NOM fouling—high flux (16.9 μm/s), low crossflow velocity (4.0 cm/s), and high Ca^{2+} concentration (1.0 m*M*)—the membrane is covered with a dark, thick layer of NOM (Figure 4a). Under more favorable hydrodynamic conditions, the fouling layer is less dense and a difference in thickness along the membrane channel can be noticed (Figure 4b). The latter observation is attributed to the local nature — i.e., dependence on the location along the filtration channel — of fouling/cake layer buildup in crossflow membrane filtration [17]. Lastly, under favorable hydrodynamic and chemical conditions — low initial flux (5.6 μm/s), high crossflow velocity (40.4 cm/s), and low Ca^{2+} concentration (0.1 m*M*) — the accumulation of NOM on the membrane surface is negligible (Figure 4c). Despite the fact that the membrane snapshots, which were taken at the end of the runs, display the fouling behavior at different cumulative permeate volumes, the qualitative results in Figure 4 are in accord with the corresponding flux decline behavior presented earlier in Figures 1–3.

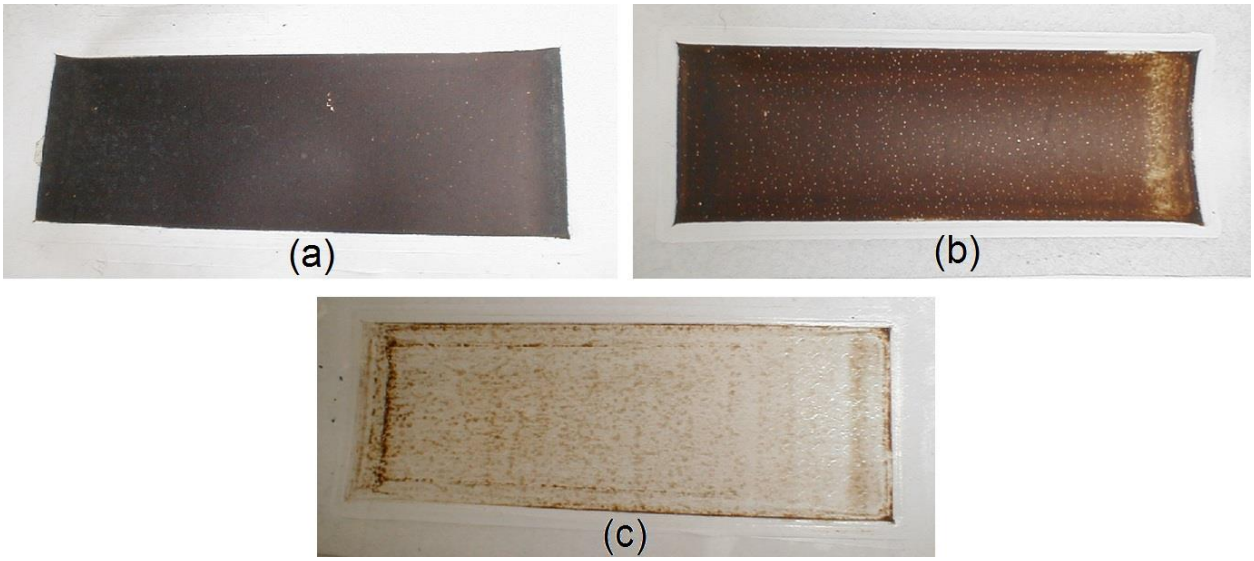

Figure 4. Snapshots of fouled membranes taken at the end of the fouling run.
Snapshots represent the following conditions: (a) initial permeate flux of 16.9 μm/s, crossflow velocity of 4.0 cm/s, Ca^{2+} concentration of 1.0 m*M*; (b) initial permeate flux of 11.3 μm/s, crossflow velocity of 12.1 cm/s, Ca^{2+} concentration of 0.3 m*M*; (c) initial permeate flux of 5.6 μm/s, crossflow velocity of 40.4 cm/s, Ca^{2+} concentration of 0.1 m*M*. The following conditions were maintained during the fouling experiments: 1.0 m*M* $NaHCO_3$, total ionic strength of 10 m*M* (adjusted by adding NaCl), pH 8.0±0.1, and temperature of 25 °C.

The amount of mass deposited on the membrane surface can be quantified gravimetrically after removing the fouling layer from the membrane at the end of the fouling run [1]. Figure 5 clearly shows that all three parameters, namely the initial permeate flux, the crossflow velocity, and the calcium ion concentration, affect the amount of deposited NOM. These results agree with the corresponding flux decline data and corroborate our hypothesis that formation of the NOM fouling and the resulting permeate flux behavior are determined by the coupled influence of hydrodynamic and chemical interactions. However, as previously discussed, the extent of fouling is affected not only by the amount of NOM deposited but also by the fouling layer structure, which is significantly influenced by specific chemical interactions. The coupled influence of chemical and hydrodynamic interactions will be a subject of further discussion in the following sections.

3.3.2 The Coupled Effects

The preceding results demonstrated that NOM accumulation at the membrane surface and the resulting fouling are controlled by the combined influence of hydrodynamic (initial permeate flux and crossflow rate) and chemical (Ca^{2+} concentration) conditions. The combined influence of the initial permeate flux, crossflow rate, and calcium ion concentration on the cumulative permeate volume (after 48 hours of filtration) is illustrated in Figure 6. Fouling is enhanced at higher initial permeate flux, elevated calcium ion concentration, and lower crossflow rate, thus resulting in reduced membrane productivity (expressed as cumulative permeate volume). These results provide the basis for optimization of operational parameters for fouling control as discussed in Section 3.5.

The hydrodynamic and chemical interactions that govern NOM fouling of crossflow NF systems are coupled. At a given crossflow velocity, the rate of NOM deposition on the membrane surface is governed by a delicate balance between permeation drag (controlled by the permeate flux) and the electrostatic repulsive force between the negatively charged NOM and the membrane surface. Where divalent cations are absent or in low concentrations, the NOM macromolecules are highly charged and NOM deposition on the membrane surface and subsequent fouling can occur only at high initial permeate flux. As the calcium ion concentration is increased, the charge on the NOM macromolecules can be significantly reduced as calcium binds to NOM carboxyl function groups, and so NOM deposition and subsequent fouling take place at even at relatively low permeate fluxes. In addition to the effect of calcium ion on the charge of NOM, calcium ions also form bridges within the deposited NOM and form a compact and highly resistant fouling layer (discussed in Section 3.2).

Figure 5. Effect of initial flux (J_0) and crossflow velocity (U_{XF}) on the deposited NOM mass on the membrane (expressed as mass per unit membrane surface area per permeate volume).

Results are shown for three calcium ion concentrations: (a) 0.1 m*M*, (b) 0.3 m*M*, and (c) 1.0 m*M*. The following conditions were maintained during the fouling experiments: 1.0 m*M* $NaHCO_3$, total ionic strength of 10 m*M* (adjusted by adding NaCl), pH 8.0±0.1, and temperature of 25 °C.

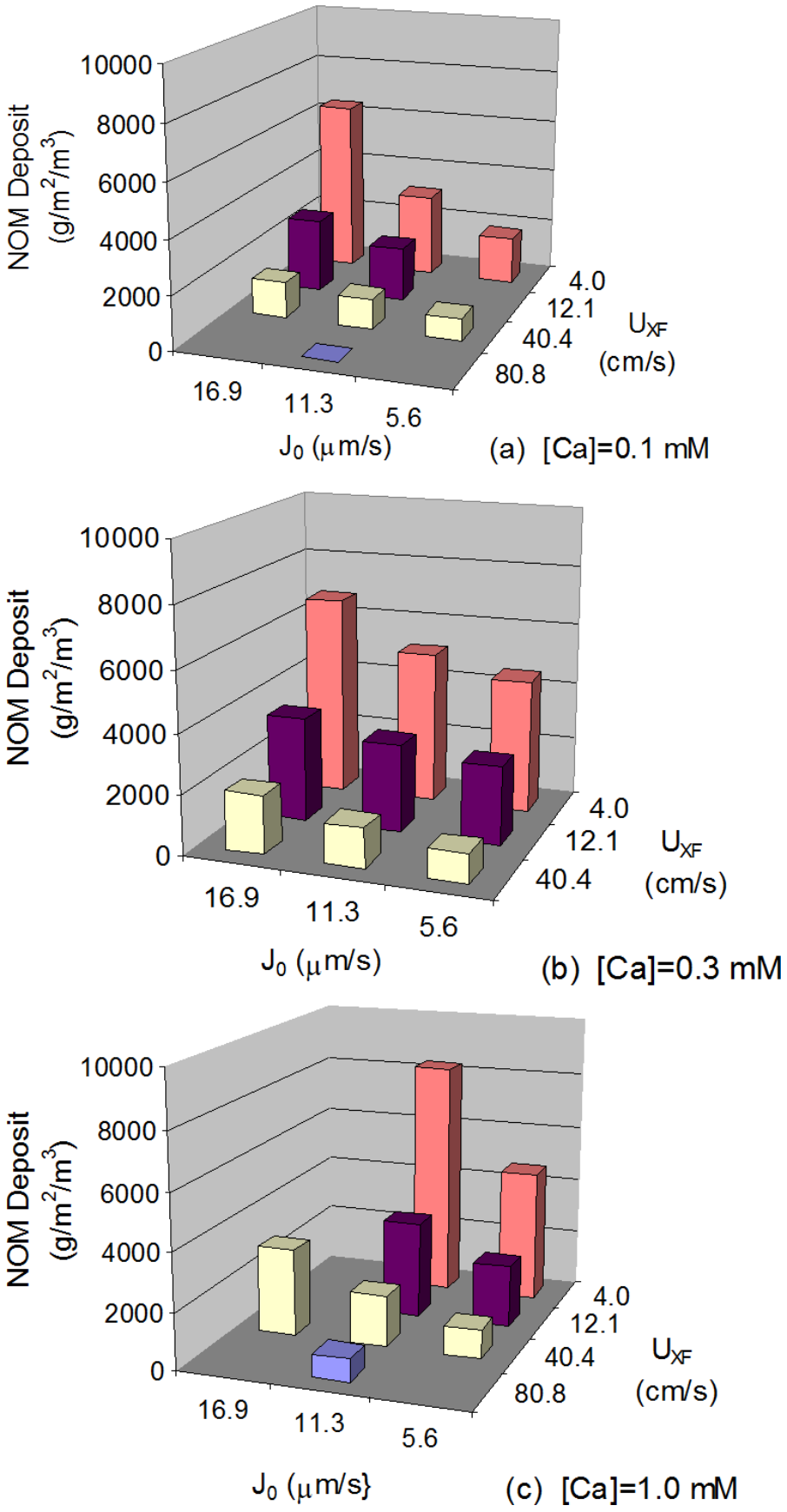

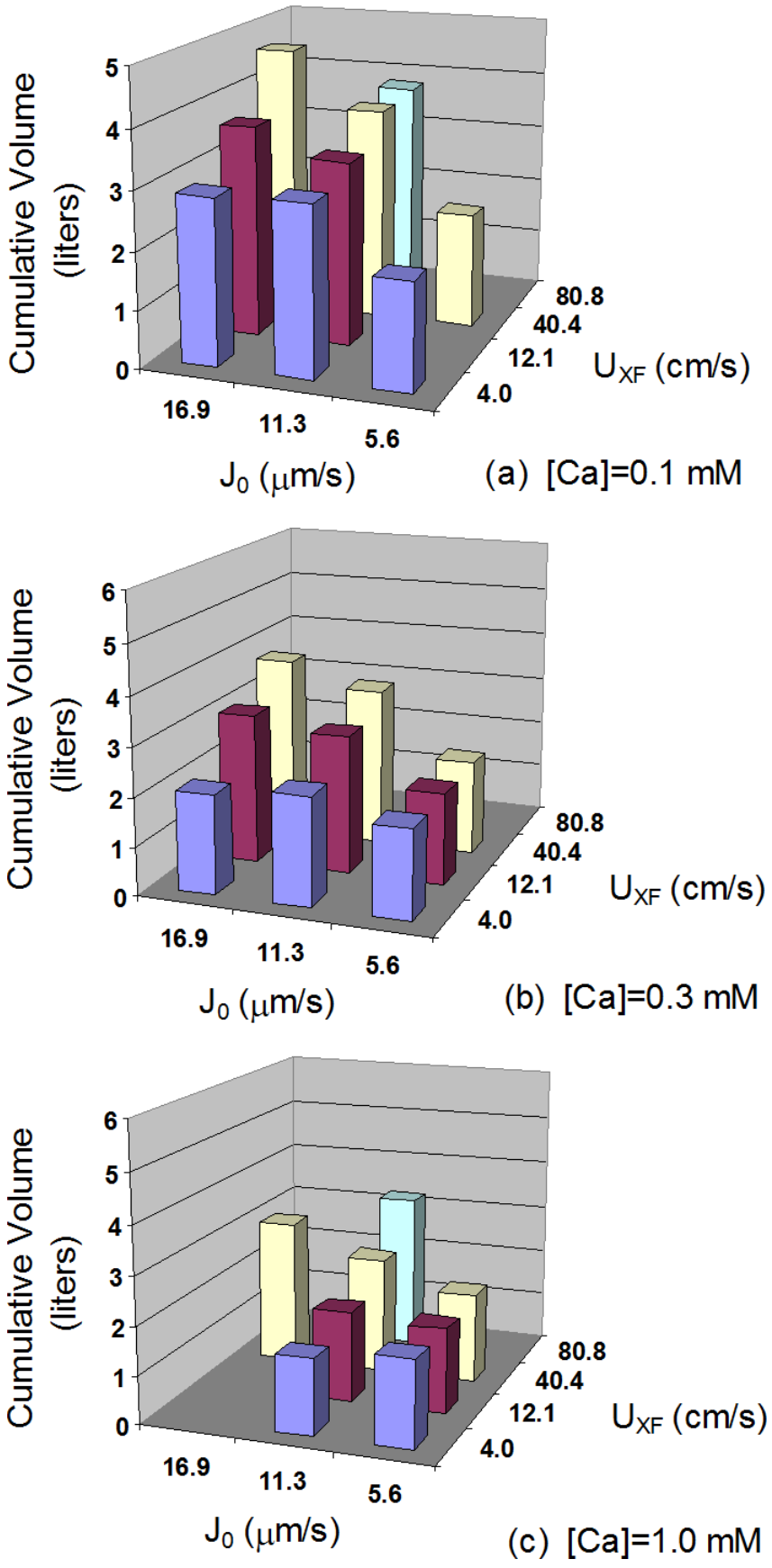

Figure 6. Effect of initial flux (J_0) and crossflow velocity (U_{XF}) on the obtained cumulative permeate volume (after 48 hours of filtration).

Results are shown for three calcium ion concentrations: (a) 0.1 m*M*, (b) 0.3 m*M*, and (c) 1.0 m*M*. The following conditions were maintained during the fouling experiments: 1.0 m*M* $NaHCO_3$, total ionic strength of 10 m*M* (adjusted by adding NaCl), pH 8.0±0.1, and temperature of 25 °C.

The hydrodynamic and chemical interactions involved in NOM fouling are also coupled via the influence of initial permeate flux and crossflow on the accumulation of the rejected Ca^{2+} ions near the membrane surface (the so-called concentration polarization). At higher initial flux (or permeation drag), the concentration of rejected Ca^{2+} at the membrane surface increases due to concentration polarization, thus enhancing fouling by Ca-NOM complex formation. Likewise, low crossflow rates result in elevated concentration of rejected Ca^{2+} at the membrane surface due to enhanced concentration polarization, which also enhances fouling.

3.3.3 The Critical Flux

The strong dependence of permeate flux on applied pressure (permeation drag) led to the critical-flux concept [18], which is based on the idea that there exists a pressure (and therefore initial flux) below which fouling (or flux decline) does not occur. Recent investigations on fouling during crossflow membrane filtration suggest that the critical flux is also dependent on the crossflow velocity [11, 19, 20]. This dependence of the critical flux on crossflow velocity is clearly observed for our NOM fouling results (Figures 1 and 2). At an initial flux of 5.6 μm/s, there is no flux decline at a crossflow velocity of 40.4 cm/s (Figure 1c or 1f), while a slight flux decline is observed at the lowest crossflow velocity of 4.0 cm/s (Figure 1a or 1d). The critical flux is higher when the crossflow velocity is increased, as evidenced by the very small flux decline at an initial flux of 11.3 μm/s and a crossflow velocity of 80.8 cm/s (Figure 2a). It is important to note that, in addition to crossflow rate and initial flux, the critical flux is also highly dependent on the Ca^{2+} concentration. This is demonstrated by the results in Figure 2, where at 1.0 m*M* Ca^{2+} (Figure 2c) the flux declined by 25 percent during the 50-hour run, whereas the flux decline was negligible at 0.1 m*M* Ca^{2+} (Figure 2a). Hence, the critical flux in NOM fouling is determined by the combined influence of chemical (divalent ion concentration) and physical/hydrodynamic conditions (initial flux and crossflow rate), and optimization of these chemical and physical parameters will determine the conditions below which membrane filtration can be realized at a constant flux and pressure.

3.4 Rejection of Calcium Ions and NOM

The NF membrane rejection of TDS, NOM, and Ca^{2+} was determined during the various fouling experiments discussed earlier. TDS rejection was in the range of 80 to 96 percent, depending on operational conditions. For a given initial permeate flux, TDS rejection increased with increasing crossflow velocity due to reduced concentration polarization, which results in lower TDS membrane concentration. The observed trend of TDS rejection as a function of initial permeate flux was not obvious. On one hand, the rejection should increase as the initial flux increases due to the so-called “dilution effect.” However, as the initial permeate rate increases, fouling becomes more severe and this generally results in lower salt rejection. The dilution effect is more important at higher crossflow velocities where fouling is less pronounced. Rejection decreased with increasing calcium concentration, an expected behavior from a negatively charged membrane such as the NF-70. For this type of membrane, salts with higher valence

counter-ions result in reduced Donnan (charge) exclusion and hence lower TDS rejection. Rejection of Ca^{2+} was relatively high, in the range of 94–99 percent, with no definite trend regarding the hydrodynamic and chemical conditions. It should be noted that some variability is expected since the permeate calcium concentration is at the lower range of the ion-specific electrode detection limit (approximately 5×10^{-6} *M*).

The rejection of NOM, as determined by UV absorbance, was 95–99 percent throughout the 50-hour run, with slight dependence on hydrodynamic and chemical conditions. For the low initial flux (5.6 μm/s) runs, rejection of NOM was 98–99 percent, but for the higher initial fluxes (11.3 and 16.9 μm/s) rejection decreased with time as NOM accumulated at the membrane surface to cause progressive fouling. Rejection values determined by TOC (93–95%) were slightly lower than those obtained by UV absorbance. This observation is not surprising in light of the fact that the UV absorbance at 254 nm is attributed mainly to absorption by aromatic/hydrophobic compounds [5, 13], whereas TOC measures the total concentration of carbon-containing molecules. Although an attempt was made to remove low-molecular-weight NOM fractions, it is clear that the model NOM used still contained a fraction of the smaller molecules, which are expected to have lower separation rates.

3.5 Optimization of Operational Parameters for Fouling Control

Preventing or reducing membrane fouling will cut the cost and increase the ease of membrane-based plant operation, as operational parameters (i.e., initial permeate flux and crossflow velocity) are directly related to energy consumption. Because operational parameters should enable high product water flux and yet minimize membrane fouling and operational costs, they need to be optimized. Higher applied pressure increases product water flux but it also increases energy demand and promotes membrane fouling. Increasing crossflow rate reduces membrane fouling but it is also associated with an increase in operational cost.

When considering fouling and the resulting flux decline, the performance of a membrane system over time can be assessed by the average product water flux

$$J_{avg} = \frac{1}{t_f}\int_0^{t_f} J dt \qquad (1)$$

where J is the time dependent flux and t_f is the total filtration time. The operational cost for a membrane system is proportional to the power used to run the membrane system. For a crossflow system, like the one used in this investigation, the power is given by

$$Power = Q\Delta P \qquad (2)$$

where Q is the crossflow rate and ΔP is the applied pressure. In this equation we neglect any frictional head loss in the module and assume negligible recovery, as the permeate flow is much smaller that the crossflow. Using

$$U_{XF} = \frac{Q}{A_{XF}} \tag{3}$$

$$J_0 = \frac{\Delta P}{\mu R_m} \tag{4}$$

it follows that

$$Power \propto U_{XF} J_0 \tag{5}$$

Here, U_{XF} is the crossflow velocity, A_{XF} is the channel cross-sectional area in the flow direction, J_0 is the initial permeate flux, μ is the solution viscosity, and R_m is the membrane resistance.

Variations of the average product water fluxes (J_{avg}) over the total filtration time (t_f = 50 hours) with the product $U_{XF}J_0$ (the power demand) are illustrated in Figure 7. The straight dashed lines represent the average flux in absence of any fouling, that is, when the initial flux J_0 is maintained throughout the 50-hour run. The experimental points (joined by the solid lines) indicate the actual average fluxes obtained at different applied pressures and crossflow velocities. These results are shown for three different calcium ion concentrations in Figures 7a–7c. We note that, in each of these figures, the straight (dashed) lines (average of the initial flux) obtained at different crossflow velocities are parallel to each other. In other words, each of these lines indicates that the average initial flux increases linearly with increased operating pressure. The experimental average fluxes at a fixed crossflow velocity, however, are considerably less than the corresponding average initial fluxes. The difference between the two becomes greater at higher pressures. This is due to the enhanced fouling at higher pressures, where the enhanced permeation drag results in a higher propensity for NOM accumulation on the membranes. Traversing the figures from left to right, we note that the extent of fouling becomes smaller (the deviation between the average initial flux and the experimental average flux decreases), indicating that higher crossflow velocities lower the extent of fouling. The trends are similar in Figures 7a–7c, although it is clear that the extent of fouling increases with increasing calcium ion concentration. Indeed, for the highest calcium concentration (1.0 m*M*), the fouling is so severe at the two lower crossflow velocities, that hardly any improvement in the average flux could be achieved by increasing the operating pressure.

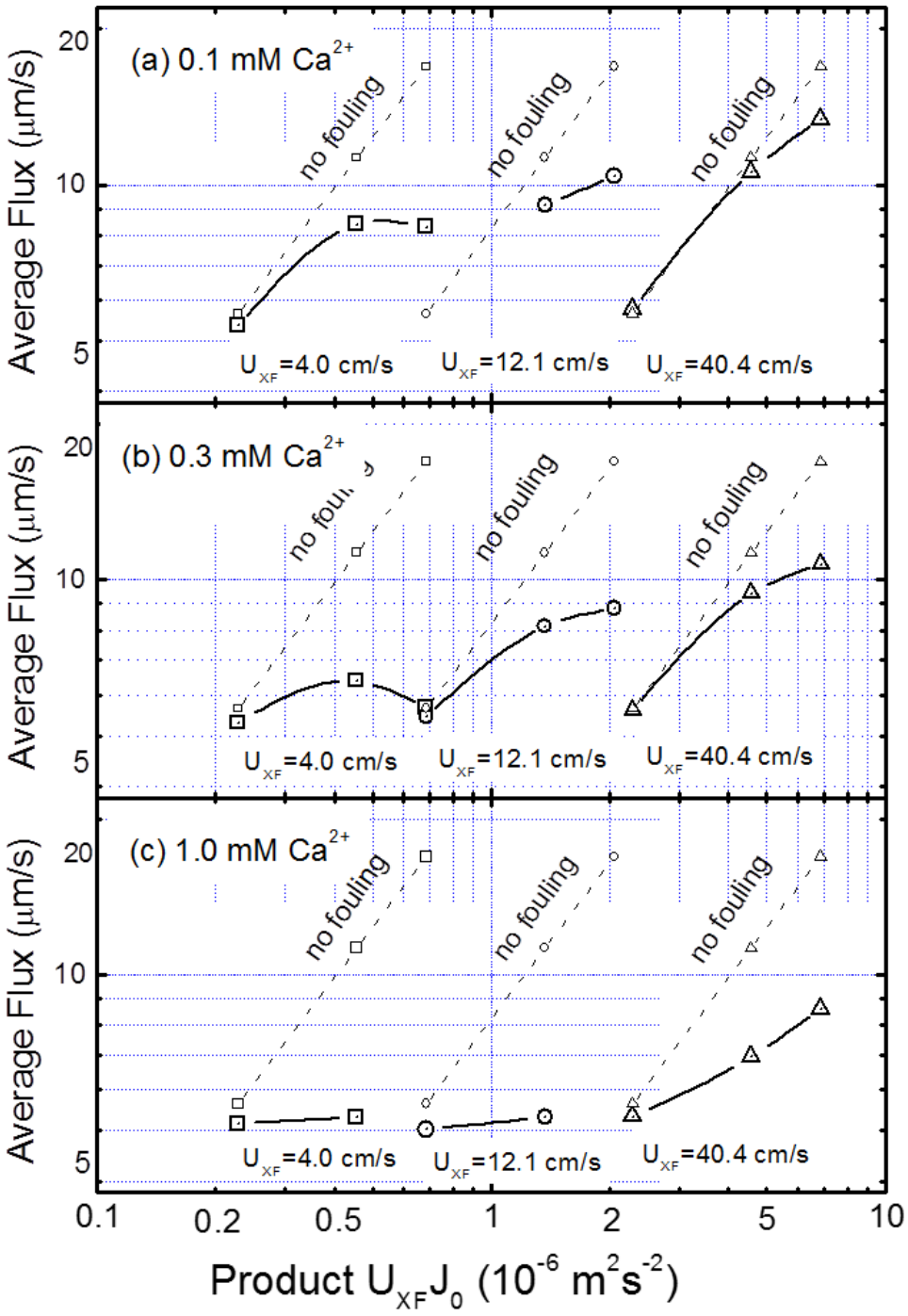

Figure 7. Average water flux J_{avg} (calculated using Eq. (1) for 50 hours operational time) as a function of the product $U_{XF}J_0$.

The dashed linear lines represent a constant flux versus time condition (i.e., no fouling, J_0) so that the connected data points are of the initial flux for each crossflow rate. The experimental points (connected with solid line) are lower than the linear, no-fouling lines and the difference is attributed to fouling. Results are shown for three crossflow velocities (indicated next to each curve) and three calcium ion concentrations: (a) 0.1 m*M*, (b) 0.3 m*M*, and (c) 1.0 m*M*. The following conditions were maintained during the fouling experiments: 1.0 m*M* $NaHCO_3$, total ionic strength of 10 m*M* (adjusted by adding NaCl), pH 8.0±0.1, and temperature of 25 °C.

The information given in Figure 7 can serve as a facile means for locating the regimes of operating conditions that would minimize fouling and maximize productivity. The cost of increasing the crossflow velocity (flow rate) and pressure head both can be expressed in terms of the total pumping cost. The cost of increasing the flow rate at a fixed head is, however, much less than the corresponding cost of increasing the pressure head at a constant flow rate. It is therefore clearly discernable that the cost of increasing crossflow velocity would be considerably lower than the corresponding cost of increasing the operating pressure. Hence, it would be reasonable to operate the filtration process at higher crossflow velocities to minimize fouling. For a given crossflow velocity, lowering the operating pressure would lead to less fouling. Although the initial fluxes for lower operating pressures will be less, increasing pressure may not significantly enhance the average experimental fluxes over a long filtration time. Provided we have a mathematical model for predicting the extent of transient flux decline caused by membrane fouling, the above information can be generalized and applied toward optimization of the operating conditions that would lead to minimal membrane fouling.

4 CONCLUSION

Natural organic matter (NOM) fouling of NF membranes is governed by the combined influence of initial permeate flux (or applied pressure), crossflow velocity, and divalent (calcium) ion concentration. Permeation drag (controlled by permeate flux) and calcium binding to NOM are the major cause for the observed rapid flux decline. An increase in crossflow velocity (shear rate) lessens these effects by reducing NOM deposition on the membrane surface and arresting the growth of the NOM fouling layer. The reported results clearly demonstrate the coupling between the hydrodynamic (permeation drag and shear rate) and chemical (Ca-NOM complexation) interactions that are involved in NOM fouling of crossflow NF systems. It is proposed that, for a given solution composition, proper choice of operational parameters (initial flux and crossflow rate) can improve membrane performance and reduce operating costs by minimizing membrane fouling.

REFERENCES

1. Hong, S.K. and M. Elimelech, Chemical and physical aspects of natural organic matter (NOM) fouling of nanofiltration membranes. *J. Membr. Sci.*, 132 (1997) 159–181.
2. Visvanathan, C., B.D. Marsono, and B. Basu, Removal of THMP by nanofiltration: Effects of interference parameters. *Water Res.*, 32 (1998) 3527–3538.
3. Manttari, M., et al., Fouling effects of polysaccharides and humic acid in nanofiltration. *J. Membr. Sci.*, 165 (2000) 1–17.
4. Wei, W., and A.L. Zydney, Humic acid fouling during ultrafiltration. *Environ. Sci. Technol.*, 34 (2000) 5043–5050.

5. Cho, J.W., G. Amy, and J. Pellegrino, Membrane filtration of natural organic matter: comparison of flux decline, NOM rejection, and foulants during filtration with three UF membranes. *Desalination*, 127 (2000) 283–298.

6. Jeantet, R., J. Rodriguez, and A. Garem, Nanofiltration of sweet whey by spiral wound organic membranes: Impact of hydrodynamics. *Lait*, 80 (2000) 155–163.

7. Wei, W., and A.L. Zydney, Effects of solution environment on humic acid fouling during microfiltration. *Desalination*, 122 (1999) 63–76.

8. Braghetta, A., F.A. DiGiano, and W.P. Ball, NOM accumulation at NF membrane surface: Impact of chemistry and shear. *J. Environ. Eng.-ASCE*, 124 (1998) 1087–1098.

9. Vrijenhoek, E.M., S. Hong, and M. Elimelech, Influence of membrane surface properties on initial rate of colloidal fouling of reverse osmosis and nanofiltration membranes. *J. Membrane Sci.*, 188 (2001) 115–128.

10. Cho, J.W., G. Amy, and J. Pellegrino, Membrane filtration of natural organic matter: Initial comparison of rejection and flux decline characteristics with ultrafiltration and nanofiltration membranes. *Water Res.*, 33 (1999) 2517–2526.

11. Fradin, B., and R.W. Field, Crossflow microfiltration of magnesium hydroxide suspensions: determination of critical fluxes, measurement, and modelling of fouling. *Sep. Purif. Technol.*, 16 (1999) 25–45.

12. Kabsch-Korbutowicz, M., K. Majewska-Nowak, and T. Winnicki, Analysis of membrane fouling in the treatment of water solutions containing humic acids and mineral salts. *Desalination*, 126 (1999) 179–185.

13. Cho, J.W., G. Amy, and J. Pellegrino, Membrane filtration of natural organic matter: factors and mechanisms affecting rejection and flux decline with charged ultrafiltration (UF) membrane. *J. Membr. Sci.*, 164 (2000) 89–110.

14. Morel, F.M.M., and J.G. Hering, *Principles and applications of aquatic chemistry*. 1993, New York: John Wiley and Sons, Inc.

15. Zhu, X.H., and M. Elimelech, Colloidal fouling of reverse osmosis membranes: Measurements and fouling mechanisms. *Environ. Sci. Technol.*, 31 (1997) 3654–3662.

16. Song, L., and M. Elimelech, Particle deposition onto permeable surface in laminar flow. *J. Colloid Interface Sci.*, 173 (1995) 165–180.

17. Song, L., and M. Elimelech, Theory of concentration polarization in crossflow filtration. *J. Chem. Soc. Faraday Trans.*, 91 (1995) 3389.

18. Field, R.W., et al., Critical flux concept for microfiltration fouling. *J. Membrane Sci.*, 100 (1995) 259–272.

19. Manttari, M. and M. Nystrom, Critical flux in NF of high molar mass polysaccharides and effluents from the paper industry. *J. Membr. Sci.*, 170 (2000) 257–273.

20. Madaeni, S.S., A.G. Fane, and D.E. Wiley, Factors influencing critical flux in membrane filtration of activated sludge. *J. Chem. Technol. Biotechnol.*, 74 (1999) 539–543.

APPENDIX:
DATA RECORD

Data Used in Compiling Figure 1(a)

Initial Flux 5.6 μm/s		Initial Flux 11.3 μm/s		Initial Flux 16.9 μm/s	
Time (hr)	Flux (μm/s)	Time (hr)	Flux (μm/s)	Time (hr)	Flux (μm/s)
0.00583	5.7193	0.00167	11.322	0.00278	16.8998
2.00362	5.6818	3.00195	10.5728	1.99972	9.2824
4.00167	5.661	5	9.4489	3.99722	7.7756
5.99945	5.6235	7.00195	8.658	6.00167	7.0263
8.00445	5.5819	9.00305	8.0836	8.00555	6.5559
10.00555	5.5486	11.0025	7.53	10.00638	6.2313
12.00888	5.5403	13.00555	7.1429	12.00388	5.9357
14.01195	5.4737	15.00778	6.8473	14.00612	5.6943
16.01055	5.4321	17.00583	6.5393	16.01138	5.5653
18.51	5.4154	18.97112	6.3894	18.00722	5.4487
20.01445	5.661	21.00833	6.1314	20.01362	5.3197
22.00667	5.6235	22.95278	6.0356	22.01112	5.1906
24.0125	5.5819	25.16972	5.84	24.01583	5.0616
26.02028	5.5486	26.91388	5.7234	26.01528	4.9784
28.01362	5.5403	28.92195	5.6444	28.01805	4.9451
30.01388	5.4737	30.92528	5.5944	30.01305	4.8993
32.0225	5.4321	32.97612	5.482	32.01083	4.7869
34.02112	5.4154	35	5.3197	34.02222	4.7369
36.025	5.3821	37	5.2472	36.01528	4.6578
38.02112	5.3488	39	5.1655	38.01917	4.5746
40.02805	5.3114	41.1225	5.0892	40.01583	4.4913
42.02583	5.2614	42.89333	5.0283	42.02307	4.4414
44.025	5.2115	45	5.0117	44.02388	4.379
46.02723	5.1573	47.5	4.8785	46.02055	4.329
48.02555	5.1199	49.87972	4.8618	48.01638	4.2791
49.53028	5.0866			49.52917	4.2499

Data Used in Compiling Figure 1(b)

Initial Flux 5.6 μm/s		Initial Flux 11.3 μm/s		Initial Flux 16.9 μm/s	
Time (hr)	Flux (μm/s)	Time (hr)	Flux (μm/s)	Time (hr)	Flux (μm/s)
0.00195	5.661	0.00445	11.4053	0.00167	16.8998
2.00195	5.6235	2.00472	11.0723	2.0025	14.985
3.99583	5.5861	4.00612	10.656	4.00333	13.1119
6.00167	5.5611	6.00417	10.3646	6.0025	12.0296
8.00112	5.5486	8.00805	9.99	8.00362	11.0306
10.00083	5.532	10.00917	9.6986	10.005	10.3646
12.00638	5.5236	12.00417	9.2824	12.00362	9.8235
14.00917	5.5153	14.0075	8.9494	14.00417	9.3656
16.00778	5.4903	16.01195	8.7413	16.00972	8.9078
18.00945	5.482	18.01305	8.4915	18.01138	8.6996
20.0075	5.4695	20.01445	8.1835	20.00695	8.4083
22.01028	5.4612	22.0125	7.9504	22.01055	8.1668
24.01445	5.4487	24.01417	7.8213	24.015	7.9837
26.00917	5.4404	26.01472	7.6632	26.01112	7.7256
28.01138	5.4279	28.01362	7.5133	28.01612	7.6132
30.015	5.4237	30.01917	7.2844	30.01167	7.4967
32.01805	5.4154	32.01612	7.1429	32.01667	7.3343
34.01778	5.4029	34.02055	7.0263	34.02028	7.2219
36.01528	5.3904	36.01638	6.864	36.01555	7.1096
38.01388	5.3821	38.02083	6.7349	38.02278	7.043
40.01972	5.3655	40.02417	6.7183	40.0189	6.9098
42.02195	5.3405	42.02195	6.635	42.01722	6.814
44.02028	5.3238	44.02222	6.506	44.02528	6.635
46.0175	5.3238	46.02307	6.3728	46.02307	6.5559
48.02472	5.3405	48.02555	6.2604	48.01945	6.5559
49.52028	5.3322	49.53055	6.2146	49.52833	6.4893

Data Used in Compiling Figure 1(c)

Initial Flux 5.6 μm/s		Initial Flux 11.3 μm/s		Initial Flux 16.9 μm/s	
Time (hr)	Flux (μm/s)	Time (hr)	Flux (μm/s)	Time (hr)	Flux (μm/s)
0	5.6777	2.83×10^{-4}	11.40526	0.00167	16.8998
2	5.6943	2	11.15551	2.0025	15.6094
4	5.6777	3.99888	11.07226	4.00083	14.4023
6	5.6943	5.99667	10.94739	6.00055	13.6114
8	5.6444	7.99972	10.65601	8.00222	12.9454
10	5.6444	9.99917	10.44789	10.00305	12.5291
12	5.6277	12.00528	10.28139	12.00445	12.0713
14	5.6277	14.00583	10.11489	14.00695	11.6966
16	5.6277	16.00778	10.03164	16.01028	11.322
18.01	5.6235	18.00667	9.78188	18.01112	11.1139
20.01	5.6194	20.00917	9.69863	20.01112	10.7393
22.01	5.6111	22.01167	9.61538	22.00888	10.4895
24.01	5.6111	24.01167	9.44888	24.01222	10.2398
26.01	5.6027	26.08612	9.15751	26.01612	10.0316
28.01	5.5944	28.08722	9.03263	28.01388	9.8235
30.02	5.5944	30.08833	8.86613	30.01555	9.657
32.01	5.5944	32.09167	8.82451	32.01972	9.4489
34.02	5.5944	34.09222	8.65801	34.015	9.2408
36.02	5.5819	36.09195	8.57476	36.0189	9.0743
40	5.5486	38.09833	8.40826	38.02278	8.9494
42	5.5445	40.09862	8.31252	40.01805	8.7829
44	5.5403	42.10195	8.21262	42.02028	8.658
46	5.5278	44.10445	8.13353	44.02307	8.4915
48	5.5153	46.10472	8.00033	46.02555	8.2959
49.5	5.507	48.10362	7.92125	48.02888	8.196
		49.85417	7.85465	49.52528	8.1169

Data Used in Compiling Figure 1(d)

Initial Flux 5.6 μm/s		Initial Flux 11.3 μm/s		Initial Flux 16.9 μm/s	
Cum. Vol. (m^3)	J/J_0	Cum. Vol. (m^3)	J/J_0	Cum. Vol. (m^3)	J/J_0
2.44×10^{-7}	1	1.36×10^{-7}	1	3.39×10^{-7}	1
8.26×10^{-5}	0.9934	1.58×10^{-4}	0.93382	1.89×10^{-4}	0.54926
1.64×10^{-4}	0.9898	3.02×10^{-4}	0.83456	3.12×10^{-4}	0.4601
2.46×10^{-4}	0.9833	4.33×10^{-4}	0.76471	4.18×10^{-4}	0.41576
3.27×10^{-4}	0.976	5.54×10^{-4}	0.71397	5.17×10^{-4}	0.38793
4.08×10^{-4}	0.9702	6.66×10^{-4}	0.66507	6.09×10^{-4}	0.36872
4.88×10^{-4}	0.9687	7.72×10^{-4}	0.63088	6.96×10^{-4}	0.35123
5.68×10^{-4}	0.9571	8.73×10^{-4}	0.60478	7.80×10^{-4}	0.33695
6.47×10^{-4}	0.9498	9.69×10^{-4}	0.57757	8.62×10^{-4}	0.32931
7.25×10^{-4}	0.9469	0.00106	0.56434	9.41×10^{-4}	0.32241
8.03×10^{-4}	0.941	0.00115	0.54154	0.00102	0.31478
8.80×10^{-4}	0.9352	0.00124	0.53309	0.00109	0.30714
9.58×10^{-4}	0.9287	0.00131	0.51581	0.00117	0.29951
0.00103	0.9199	0.00137	0.50551	0.00124	0.29458
0.00111	0.9112	0.00141	0.49853	0.00131	0.29261
0.00119	0.9017	0.0015	0.49412	0.00138	0.2899
0.00126	0.8952	0.00158	0.48419	0.00145	0.28325
0.00133	0.8894	0.00168	0.46985	0.00152	0.2803
0.00141	0.8821	0.00176	0.46345	0.00159	0.27562
0.00148	0.8777	0.00184	0.45623	0.00166	0.27069
0.00155	0.8748	0.00191	0.4495	0.00172	0.26576
0.00162	0.8712	0.00199	0.44412	0.00179	0.26281
0.0017	0.8675	0.00202	0.44265	0.00185	0.25911
0.00177	0.8639	0.00213	0.43088	0.00191	0.25616
0.00184	0.8603	0.00214	0.42941	0.00197	0.2532
0.00189	0.8574	0.00216	0.42941	0.00202	0.25148
		0.00221	0.4239		
		0.00224	0.4239		
		0.0023	0.41949		

Data Used in Compiling Figure 1(e)

Initial Flux 5.6 μm/s		Initial Flux 11.3 μm/s		Initial Flux 16.9 μm/s	
Cum. Vol. (m^3)	J/J_0	Cum. Vol. (m^3)	J/J_0	Cum. Vol. (m^3)	J/J_0
7.95×10^{-8}	1	3.66×10^{-7}	1	2.03×10^{-7}	1
8.14×10^{-5}	0.99338	1.62×10^{-4}	0.9708	2.30×10^{-4}	0.8867
1.62×10^{-4}	0.98676	3.19×10^{-4}	0.93431	4.33×10^{-4}	0.77586
2.43×10^{-4}	0.98235	4.70×10^{-4}	0.90876	6.14×10^{-4}	0.71182
3.23×10^{-4}	0.98015	6.17×10^{-4}	0.87591	7.80×10^{-4}	0.65271
4.02×10^{-4}	0.97721	7.59×10^{-4}	0.85036	9.34×10^{-4}	0.6133
4.82×10^{-4}	0.97574	8.96×10^{-4}	0.81387	0.00108	0.58128
5.62×10^{-4}	0.97426	0.00103	0.78467	0.00122	0.55419
6.41×10^{-4}	0.96985	0.00116	0.76642	0.00135	0.52709
7.20×10^{-4}	0.96838	0.00128	0.74453	0.00148	0.51478
7.99×10^{-4}	0.96618	0.0014	0.71752	0.0016	0.49754
8.78×10^{-4}	0.96471	0.00152	0.69708	0.00172	0.48325
9.57×10^{-4}	0.9625	0.00163	0.68577	0.00184	0.47241
0.00104	0.96103	0.00174	0.6719	0.00195	0.45714
0.00111	0.95882	0.00185	0.65876	0.00206	0.45049
0.00119	0.95809	0.00196	0.63869	0.00217	0.4436
0.00127	0.95662	0.00206	0.62628	0.00228	0.43399
0.00135	0.95441	0.00216	0.61606	0.00238	0.42734
0.00143	0.95221	0.00226	0.60182	0.00248	0.42069
0.0015	0.95074	0.00236	0.59051	0.00259	0.41675
0.00158	0.94779	0.00246	0.58905	0.00269	0.40887
0.00166	0.94338	0.00256	0.58175	0.00279	0.4032
0.00174	0.94044	0.00265	0.57044	0.00288	0.39261
0.00181	0.94044	0.00274	0.55876	0.00298	0.38793
0.00189	0.94338	0.00283	0.54891	0.00307	0.38793
0.00195	0.94191	0.0029	0.54489	0.00314	0.38399

Data Used in Compiling Figure 1(f)

Initial Flux 5.6 μm/s		Initial Flux 11.3 μm/s		Initial Flux 16.9 μm/s	
Cum. Vol. (m^3)	J/J_0	Cum. Vol. (m^3)	J/J_0	Cum. Vol. (m^3)	J/J_0
1.25×10^{-7}	1	2.30×10^{-8}	1	2.03×10^{-7}	1
8.21×10^{-5}	1.00293	1.63×10^{-4}	0.9781	2.35×10^{-4}	0.92365
1.64×10^{-4}	1	3.23×10^{-4}	0.9708	4.51×10^{-4}	0.85222
2.46×10^{-4}	1.00293	4.81×10^{-4}	0.95985	6.53×10^{-4}	0.80542
3.28×10^{-4}	0.99413	6.37×10^{-4}	0.93431	8.44×10^{-4}	0.76601
4.09×10^{-4}	0.99413	7.89×10^{-4}	0.91606	0.00103	0.74138
4.90×10^{-4}	0.9912	9.39×10^{-4}	0.90146	0.00121	0.71429
5.71×10^{-4}	0.9912	0.00109	0.88686	0.00138	0.69212
6.53×10^{-4}	0.9912	0.00123	0.87956	0.00154	0.66995
7.34×10^{-4}	0.99047	0.00137	0.85766	0.0017	0.65764
8.15×10^{-4}	0.98974	0.00151	0.85036	0.00186	0.63547
8.96×10^{-4}	0.98827	0.00165	0.84307	0.00202	0.62069
9.77×10^{-4}	0.98827	0.00179	0.82847	0.00216	0.60591
0.00106	0.9868	0.00193	0.80292	0.00231	0.5936
0.00114	0.98534	0.00206	0.79197	0.00245	0.58128
0.00122	0.98534	0.00219	0.77737	0.00259	0.57143
0.0013	0.98534	0.00232	0.77372	0.00273	0.55911
0.00138	0.98534	0.00244	0.75912	0.00287	0.5468
0.00146	0.98314	0.00257	0.75182	0.003	0.53695
0.00153	0.97727	0.00269	0.73723	0.00313	0.52956
0.00162	0.97654	0.00281	0.72883	0.00326	0.5197
0.0017	0.97581	0.00293	0.72007	0.00338	0.51232
0.00178	0.97361	0.00305	0.71314	0.00351	0.50246
0.00186	0.97141	0.00317	0.70146	0.00363	0.49089
0.00194	0.96994	0.00328	0.69453	0.00375	0.48498
0.002	0.96848	0.00338	0.68869	0.00383	0.4803

Data Used in Compiling Figure 2(a)

Crossflow Velocity = 4.0 cm/s		Crossflow Velocity = 12.1 cm/s		Crossflow Velocity = 40.4 cm/s		Crossflow Velocity = 80.8 cm/s	
Cum. Vol. (m^3)	J/J_0	Cum. Vol. (m^3)	J/J_0	Cum. Vol. (m^3)	J/J_0	Cum. Vol. (m^3)	J/J_0
6.85×10^{-8}	1	0	1	4.55×10^{-7}	1	0	1
1.63×10^{-4}	0.98901	1.63×10^{-4}	0.98901	1.64×10^{-4}	0.99634	1.64×10^{-4}	1.0059
3.23×10^{-4}	0.95971	3.24×10^{-4}	0.98535	3.27×10^{-4}	0.99267	3.26×10^{-4}	0.9971
4.77×10^{-4}	0.92674	4.85×10^{-4}	0.9707	4.89×10^{-4}	0.98901	4.89×10^{-4}	0.9971
6.26×10^{-4}	0.89011	6.42×10^{-4}	0.94872	6.51×10^{-4}	0.98535	6.51×10^{-4}	0.9941
7.70×10^{-4}	0.86813	7.95×10^{-4}	0.92674	8.12×10^{-4}	0.98168	8.11×10^{-4}	0.9801
9.10×10^{-4}	0.83883	9.45×10^{-4}	0.9011	9.72×10^{-4}	0.97436	9.71×10^{-4}	0.9801
0.00105	0.82051	0.00109	0.88645	0.00113	0.9707	0.00113	0.9801
0.00118	0.79487	0.00123	0.86081	0.00129	0.96337	0.00129	0.9713
0.00131	0.77289	0.00137	0.84615	0.00145	0.95971	0.00145	0.9743
0.00143	0.75458	0.00151	0.82418	0.00159	0.95238	0.00161	0.9743
0.00155	0.73626	0.00164	0.80586	0.00177	0.94505	0.00177	0.9743
0.00167	0.71722	0.00178	0.79121	0.0019	0.93773	0.00193	0.9713
0.00179	0.7011	0.0019	0.78022	0.00207	0.93407	0.00208	0.9684
0.0019	0.68681	0.00203	0.76557	0.00223	0.92674	0.0023	0.9625
0.00201	0.67143	0.00216	0.75458	0.00236	0.92308	0.00242	0.9713
0.00212	0.65971	0.00228	0.73626	0.00252	0.91575	0.00255	0.9573
0.00223	0.64542	0.0024	0.72711	0.00267	0.90991	0.00271	0.9545
0.00234	0.63553	0.00252	0.71429	0.00282	0.9032	0.00287	0.9517
0.00244	0.62271	0.00263	0.70549	0.00297	0.89654	0.00302	0.9489
0.00255	0.61465	0.00275	0.69707	0.00317	0.89377	0.00317	0.9461
0.00266	0.60659	0.00286	0.68278	0.00326	0.89011	0.00331	0.9419
0.00274	0.59524	0.00297	0.67839	0.0034	0.88278	0.00347	0.9419
0.00283	0.58681	0.00308	0.6685	0.00355	0.87546	0.00361	0.9368
0.00293	0.57839	0.00319	0.66264	0.00369	0.87179	0.00378	0.9338
0.00302	0.57399	0.0033	0.65531	0.00383	0.86447	0.00387	0.9368
		0.00332	0.65128			0.00395	0.9279

Data Used in Compiling Figure 2(b)

Crossflow Velocity = 4.0 cm/s		Crossflow Velocity = 12.1 cm/s		Crossflow Velocity = 40.4 cm/s	
Cum. Vol. (m^3)	J/J_0	Cum. Vol. (m^3)	J/J_0	Cum. Vol. (m^3)	J/J_0
1.36×10^{-7}	1	3.66×10^{-7}	1	2.30×10^{-8}	1
1.58×10^{-4}	0.93382	1.62×10^{-4}	0.9708	1.63×10^{-4}	0.9781
3.02×10^{-4}	0.83456	3.19×10^{-4}	0.93431	3.23×10^{-4}	0.9708
4.33×10^{-4}	0.76471	4.70×10^{-4}	0.90876	4.81×10^{-4}	0.95985
5.54×10^{-4}	0.71397	6.17×10^{-4}	0.87591	6.37×10^{-4}	0.93431
6.66×10^{-4}	0.66507	7.59×10^{-4}	0.85036	7.89×10^{-4}	0.91606
7.72×10^{-4}	0.63088	8.96×10^{-4}	0.81387	9.39×10^{-4}	0.90146
8.73×10^{-4}	0.60478	0.00103	0.78467	0.00109	0.88686
9.69×10^{-4}	0.57757	0.00116	0.76642	0.00123	0.87956
0.00106	0.56434	0.00128	0.74453	0.00137	0.85766
0.00115	0.54154	0.0014	0.71752	0.00151	0.85036
0.00124	0.53309	0.00152	0.69708	0.00165	0.84307
0.00131	0.51581	0.00163	0.68577	0.00179	0.82847
0.00137	0.50551	0.00174	0.6719	0.00193	0.80292
0.00141	0.49853	0.00185	0.65876	0.00206	0.79197
0.0015	0.49412	0.00196	0.63869	0.00219	0.77737
0.00158	0.48419	0.00206	0.62628	0.00232	0.77372
0.00168	0.46985	0.00216	0.61606	0.00244	0.75912
0.00176	0.46345	0.00226	0.60182	0.00257	0.75182
0.00184	0.45623	0.00236	0.59051	0.00269	0.73723
0.00191	0.4495	0.00246	0.58905	0.00281	0.72883
0.00199	0.44412	0.00256	0.58175	0.00293	0.72007
0.00202	0.44265	0.00265	0.57044	0.00305	0.71314
0.00213	0.43088	0.00274	0.55876	0.00317	0.70146
0.00214	0.42941	0.00283	0.54891	0.00328	0.69453
0.00216	0.42941	0.0029	0.54489	0.00338	0.68869
0.00221	0.4239				
0.00224	0.4239				
0.0023	0.41949				

Data Used in Compiling Figure 2(c)

Crossflow Velocity = 4.0 cm/s		Crossflow Velocity = 12.1 cm/s		Crossflow Velocity = 40.4 cm/s		Crossflow Velocity = 80.8 cm/s	
Cum. Vol. (m^3)	J/J_0	Cum. Vol. (m^3)	J/J_0	Cum. Vol. (m^3)	J/J_0	Cum. Vol. (m^3)	J/J_0
2.74×10^{-7}	1	2.51×10^{-7}	1	4.57×10^{-7}	1	0	1
1.43×10^{-4}	0.7336	1.51×10^{-4}	0.8394	1.56×10^{-4}	0.9015	1.46×10–4	0.9831
2.52×10^{-4}	0.5945	2.79×10^{-4}	0.7161	2.99×10^{-4}	0.8285	3.05×10^{-4}	0.9654
3.43×10^{-4}	0.5204	3.91×10^{-4}	0.6431	4.31×10^{-4}	0.7774	4.60×10^{-4}	0.9338
4.25×10^{-4}	0.4763	4.92×10^{-4}	0.5876	5.55×10^{-4}	0.7336	6.11×10^{-4}	0.9169
5.01×10^{-4}	0.4423	5.85×10^{-4}	0.5504	6.73×10^{-4}	0.7029	7.59×10^{-4}	0.8963
5.72×10^{-4}	0.4208	6.74×10^{-4}	0.5277	7.87×10^{-4}	0.6774	9.04×10^{-4}	0.8765
6.39×10^{-4}	0.4007	7.59×10^{-4}	0.5047	8.97×10^{-4}	0.6544	0.00105	0.8618
7.04×10^{-4}	0.385	8.40×10^{-4}	0.4748	1.00×10^{-3}	0.6361	0.00119	0.8478
7.66×10^{-4}	0.3752	9.14×10^{-4}	0.4551	0.00111	0.6161	0.00132	0.8419
8.27×10^{-4}	0.3639	9.65×10^{-4}	0.4464	0.00121	0.6033	0.00146	0.825
8.86×10^{-4}	0.3511	0.00105	0.4314	0.0013	0.5876	0.00159	0.8191
9.43×10^{-4}	0.3438	0.00113	0.4164	0.0014	0.5763	0.00172	0.8103
9.99×10^{-4}	0.3365	0.0012	0.4015	0.00149	0.5617	0.00185	0.7993
0.00105	0.3296	0.00126	0.392	0.00158	0.5489	0.00198	0.7904
0.00111	0.3208	0.00133	0.3836	0.00167	0.5361	0.00211	0.7816
0.00116	0.3168	0.00139	0.3785	0.00176	0.5219	0.00224	0.7728
0.00121	0.3124	0.00145	0.3741	0.00185	0.5146	0.00236	0.761
0.00126	0.3069	0.00151	0.3639	0.00193	0.5047	0.00249	0.7581
0.00131	0.304	0.00157	0.3591	0.00201	0.4978	0.00261	0.7471
0.00136	0.3011	0.00163	0.3536	0.00209	0.4894	0.00273	0.7471
0.00141	0.2967	0.00169	0.3496	0.00217	0.4792	0.00285	0.7412
0.00146	0.2938	0.00177	0.3453	0.00225	0.4734	0.00297	0.7331
0.00151	0.288	0.0018	0.3409	0.00233	0.4635	0.00309	0.7331
0.00156	0.285	0.00186	0.3394	0.0024	0.4577	0.00321	0.7272
0.00159	0.2825	0.00191	0.338	0.00246	0.4493	0.0033	0.7213
						0.00339	0.7154

Data Used in Compiling Figure 3(a)

Ca^{2+} Conc. = 0.1 m*M*		Ca^{2+} Conc. = 0.3 m*M*	
Time (hr)	**Flux (μm/s)**	**Time (hr)**	**Flux (μm/s)**
0	17.0246	0	16.8998
2	16.6084	2	15.6094
4	16.1921	4	14.4023
6	15.8175	6	13.6114
8.01	15.4845	8	12.9454
10.01	15.0683	10	12.5291
12	14.8601	12	12.0713
14.01	14.4855	14.01	11.6966
16.01	14.2358	16.01	11.322
17.93	14.0276	18.01	11.1139
22.34	13.4033	20.01	10.7393
24	13.2368	22.01	10.4895
25.93	12.987	24.01	10.2398
27.87	12.7789	26.02	10.0316
30.09	12.4875	28.01	9.8235
32.02	12.321	30.02	9.657
33.96	12.1961	32.02	9.4489
35.9	11.988	34.02	9.2408
38.12	11.8215	36.02	9.0743
40.05	11.6134	38.02	8.9494
41.99	11.5301	40.02	8.7829
43.93	11.322	42.02	8.658
45.87	11.2388	44.02	8.4915
48.01	10.989	46.03	8.2959
49.93	10.8225	48.03	8.196
		49.53	8.1169

Data Used in Compiling Figure 3(b)

Ca^{2+} Conc. = 0.0 m*M*		Ca^{2+} Conc. = 0.1 m*M*		Ca^{2+} Conc. = 0.3 m*M*		Ca^{2+} Conc. = 1.0 m*M*	
Time (hr)	**Flux (μm/s)**	**Time (hr)**	**Flux (μm/s)**	**Time (hr)**	**Flux (μm/s)**	**Time (hr)**	**Flux (μm/s)**
0	11.2804	0	11.375	0	11.4053	0	11.4053
2.161		1.999	11.25	2	11.0723	2	9.5738
4.161		3.998	11.2083	4.01	10.656	4	8.1668
6.16	11.1555	5.998	11.0417	6	10.3646	6	7.3343
8.16	11.1555	7.998	10.7917	8.01	9.99	8	6.7016
10.16	11.0723	9.997	10.5417	10.01	9.6986	10	6.2771
12.16	10.8641	11.997	10.25	12	9.2824	12	6.019
14.159	10.8225	13.997	10.0833	14.01	8.9494	14.01	5.7567
16.159	10.6144	15.996	9.7917	16.01	8.7413	16.01	5.4154
18.158	10.4895	17.996	9.625	18.01	8.4915	17.94	5.1906
20.158	10.3646	19.996	9.375	20.01	8.1835	19.33	5.0907
22.158	10.1149	21.996	9.1667	22.01	7.9504	21.67	4.9201
24.158	10.0316	23.995	9	24.01	7.8213	24.01	4.7494
26.157	9.8235	25.995	8.875	26.01	7.6632	26.1	4.5788
28.157	9.7403	27.994	8.7083	28.01	7.5133	27.9	4.4705
30.157	9.6154	29.994	8.5833	30.02	7.2844	30.01	4.3748
32.156	9.5321	31.994	8.375	32.02	7.1429	32.11	4.3165
34.156	9.4073	33.994	8.2708	34.02	7.0263	33.91	4.2666
36.156	9.3656	35.993	8.125	36.02	6.864	36.01	4.15
38.156	9.2824	37.993	8.025	38.02	6.7349	38.11	4.0959
40.155	9.1991	39.993	7.9292	40.02	6.7183	39.92	4.0335
42.155	9.1575	41.993	7.7667	42.02	6.635	42.02	3.9877
44.154	9.0743	43.992	7.7167	44.02	6.506	45	3.9377
46.154	9.0743	45.992	7.6042	46.02	6.3728	46	3.8878
48.154	8.9494	47.992	7.5375	48.03	6.2604	48.02	3.8711
49.154	8.8245	49.991	7.4542	49.53	6.2146	49.97	3.8545
		50.491	7.4083				

Data Used in Compiling Figure 3(c)

Ca^{2+} Conc. = 0.1 m*M*		Ca^{2+} Conc. = 0.3 m*M*		Ca^{2+} Conc. = 1.0 m*M*	
Time (hr)	**Flux (μm/s)**	**Time (hr)**	**Flux (μm/s)**	**Time (hr)**	**Flux (μm/s)**
0	5.661	0.01	5.7193	0	5.6833
2	5.636	2	5.6818	2.068	5.7958
4	5.6111	4	5.661	4.068	5.6833
6	5.5778	6	5.6235	6.068	5.6333
8.01	5.5569	8	5.5819	8.067	5.5875
10.01	5.532	10.01	5.5486	10.067	5.4875
12.01	5.5028	12.01	5.5403	12.067	5.4708
14.01	5.482	14.01	5.4737	14.066	5.4375
16	5.457	16.01	5.4321	16.066	5.3708
18	5.4404	18.01	5.4154	18.066	5.325
20	5.4196	20.01	5.3821	20.066	5.2583
22	5.4071	22.01	5.3488	22.065	5.1792
24	5.3821	24.01	5.3114	24.065	5.1792
25.62	5.3655	26.02	5.2614	26.064	5.0958
28	5.3238	28.01	5.2115	28.064	5.0792
30.01	5.2697	30.01	5.1573	30.064	5
32	5.2531	32.02	5.1199	32.064	4.95
34	5.2156	34.02	5.0866	34.063	4.9
36.01	5.1906	36.03	5.045	36.063	4.8667
38.01	5.1906	38.02	5.02	38.063	4.8333
40	5.1573	40.03	5.0033	40.062	4.7875
42.01	5.124	42.03	4.9825	42.062	4.7875
44.01	5.1573	44.03	4.9617	44.062	4.7208
46	5.124	46.03	4.9409	46.061	4.6875
48.01	5.124	48.03	4.9201	48.061	4.6583
50.01	5.0616	49.53	4.9034	49.061	4.6417

Data Used in Compiling Figure 3(d)

Ca^{2+} Conc. = 0.1 m*M*		Ca^{2+} Conc. = 0.3 m*M*		Ca^{2+} Conc. = 1.0 m*M*	
Time (hr)	**Flux (μm/s)**	**Time (hr)**	**Flux (μm/s)**	**Time (hr)**	**Flux (μm/s)**
0.01	11.3636	0	11.40526	0.01	11.4053
2.01	11.322	2	11.15551	2	10.2814
4.01	11.2804	4	11.07226	4	9.4489
6.01	11.2388	6	10.94739	6	8.8661
8.01	11.1971	8	10.65601	8.01	8.3666
10.01	11.1555	10	10.44789	10.01	8.017
12.01	11.0723	12.01	10.28139	12.01	7.7256
14.01	11.0306	14.01	10.11489	14.01	7.4634
16.01	10.9474	16.01	10.03164	16.01	7.2552
18.01	10.9058	18.01	9.88188	18.01	7.0263
19.86	10.8641	20.01	9.69863	20.01	6.8806
22.09	10.7809	22.01	9.55538	22.01	6.7016
23.89	10.7393	24.01	9.34888	24.02	6.5726
25.99	10.656	26.09	9.15751	26.02	6.4061
28.09	10.5728	28.09	9.03263	28.01	6.2604
29.89	10.4895	30.09	8.85613	30.02	6.1147
31.99	10.4063	32.09	8.82451	32.02	5.9524
34	10.3399	34.09	8.65801	34.02	5.8691
36	10.2637	36.09	8.57476	36.02	5.7567
38	10.188	38.1	8.40826	38.02	5.6777
40.83	10.1565	40.1	8.31252	40.03	5.5819
42.02	10.1149	42.1	8.21262	42.03	5.4654
43.96	10.0316	44.1	8.13353	44.02	5.3988
45.98	9.9484	46.1	8.00033	46.03	5.2864
48	9.9068	48.1	7.92125	48.02	5.2198
49.93	9.8235	49.85	7.85465	49.53	5.124

Data Used in Compiling Figure 5(a), for Ca^{2+} = 0.1 m*M*

Crossflow (cm/s)	NOM Deposit (g per m^2 of membrane per m^3 of permeate)		
	J_0 = 16.9 µm/s	J_0 = 11.3 µm/s	J_0 = 5.6 µm/s
80.8		2.362	
40.4	1,356.24	1,090.034	823.511
12.1	2,722.25	1,982.218	
4.0	6,395.13	3,072.480	1,757.908

Data Used in Compiling Figure 5(b), for Ca^{2+} = 0.3 m*M*

Crossflow (cm/s)	NOM Deposit (g per m^2 of membrane per m^3 of permeate)		
	J_0 = 16.9 µm/s	J_0 = 11.3 µm/s	J_0 = 5.6 µm/s
40.4	1,940.42	1,315.723	937.502
12.1	3,469.01	2,944.307	2,595.091
4.0	6,724.79	5,117.694	4,493.255

Data Used in Compiling Figure 5(c), for Ca^{2+} = 1.0 m*M*

Crossflow (cm/s)	NOM Deposit (g per m^2 of membrane per m^3 of permeate)		
	J_0 = 16.9 µm/s	J_0 = 11.3 µm/s	J_0 = 5.6 µm/s
80.8		782.804	
40.4	3,057.86	1,777.969	1,000.284
12.1		3,370.757	2,173.154
4.0		8,297.906	4,656.035

Data Used in Compiling Figure 6(a), for Ca^{2+} = 0.1 m*M*

Crossflow (cm/s)	Permeate Volume (L) after 48 Hours of Filtration		
	J_0 = 16.9 µm/s	J_0 = 11.3 µm/s	J_0 = 5.64 µm/s
4.0	2.88	2.93	1.86
12.1	3.65	3.19	
40.4	4.66	3.69	1.99
80.8		3.78	

Data Used in Compiling Figure 6(b), for Ca^{2+} = 0.3 m*M*

Crossflow (cm/s)	Permeate Volume (L) after 48 Hours of Filtration		
	J_0 = 16.9 µm/s	J_0 = 11.3 µm/s	J_0 = 5.64 µm/s
4.0	2.02	2.23	1.84
12.1	3.07	2.83	1.89
40.4	3.75	3.28	1.94

Data Used in Compiling Figure 6(c), for Ca^{2+} = 1.0 m*M*

Crossflow (cm/s)	Permeate Volume (L) after 48 Hours of Filtration		
	J_0 = 16.9 µm/s	J_0 = 11.3 µm/s	J_0 = 5.64 µm/s
4.0		1.56	1.79
12.1		1.86	1.75
40.4	3.00	2.40	1.85
80.8		3.23	

Data Used in Compiling Figure 7(a), for Ca^{2+} = 0.1 m*M*

Crossflow = 4.0 cm/s			Crossflow = 12.1 cm/s			Crossflow = 40.4 cm/s		
$U_{XF}J_0$ (10^{-6} m^2s^{-2})	Avg. Flux (μm/s)		$U_{XF}J_0$ (10^{-6} m^2s^{-2})	Avg. Flux (μm/s)		$U_{XF}J_0$ (10^{-6} m^2s^{-2})	Avg. Flux (μm/s)	
	Experimental	Without Fouling		Experimental	Without Fouling		Experimental	Without Fouling
0.228	5.35	5.64	0.68		5.64	2.28	5.76	5.64
0.456	8.39	11.28	1.37	9.14	11.28	4.56	10.6	11.28
0.684	8.28	16.92	2.05	10.4	16.92	6.84	13.4	16.92

Data Used in Compiling Figure 7(b), for Ca^{2+} = 0.3 m*M*

Crossflow = 4.0 cm/s			Crossflow = 12.1 cm/s			Crossflow = 40.4 cm/s		
$U_{XF}J_0$ (10^{-6} m^2s^{-2})	Avg. Flux (μm/s)		$U_{XF}J_0$ (10^{-6} m^2s^{-2})	Avg. Flux (μm/s)		$U_{XF}J_0$ (10^{-6} m^2s^{-2})	Avg. Flux (μm/s)	
	Experimental	Without Fouling		Experimental	Without Fouling		Experimental	Without Fouling
0.228	5.3	5.64	0.68	5.45	5.64	2.28	5.61	5.64
0.456	6.39	11.28	1.37	8.13	11.28	4.56	9.41	11.28
0.684	5.66	16.92	2.05	8.81	16.92	6.84	10.7	16.92

Data Used in Compiling Figure 7(c), for Ca^{2+} = 1.0 m*M*

Crossflow = 4.0 cm/s			Crossflow = 12.1 cm/s			Crossflow = 40.4 cm/s		
$U_{XF}J_0$ (10^{-6} m^2s^{-2})	Avg. Flux (μm/s)		$U_{XF}J_0$ (10^{-6} m^2s^{-2})	Avg. Flux (μm/s)		$U_{XF}J_0$ (10^{-6} m^2s^{-2})	Avg. Flux (μm/s)	
	Experimental	Without Fouling		Experimental	Without Fouling		Experimental	Without Fouling
0.228	5.16	5.64	0.68	5.03	5.64	2.28	5.33	5.64
0.456	5.3	11.28	1.37	5.31	11.28	4.56	6.96	11.28
0.684		16.92	2.05		16.92	6.84	8.6	16.92